Chemical Physics Letters 673 (2017) 68–73

Contents lists available at ScienceDirect

Chemical Physics Letters

journal homepage: www.elsevier.com/locate/cplett

Research paper

Formation, thermal decomposition and atmospheric implications of the $CF_2(OH)CF_2OONO_2$ and $CF_3CF_2OONO_2$ peroxynitrates. A theoretical study

María Paula Badenes

Instituto de Investigaciones Fisicoquímicas Teóricas y Aplicadas (INIFTA), Departamento de Química, Facultad de Ciencias Exactas, Universidad Nacional de La Plata, CONICET, Casilla de Correo 16, Sucursal 4, 1900 La Plata, Argentina

ARTICLE INFO

Article history:
Received 21 November 2016
Revised 25 January 2017
In final form 27 January 2017
Available online 8 February 2017

Keywords:
Peroxynitrates
$CF_2(OH)CF_2OONO_2$
$CF_3CF_2OONO_2$
Quantum-chemical calculations
SACM/CT calculations

ABSTRACT

A SACM/CT study of the $CF_2(OH)CF_2OO + NO_2 \rightarrow CF_2(OH)CF_2OONO_2$ and $CF_3CF_2OO + NO_2 \rightarrow CF_3CF_2OONO_2$ recombination reactions and their reverse unimolecular decomposition process was performed. The electronic energy along the reaction pathways was calculated at the G4(MP2) level. High-pressure rate coefficients of $1.53 \times 10^{-12}\,(T/300)^{0.37}$ cm^3 molecule^{-1} s^{-1} and $1.79 \times 10^{16}\,(T/300)^{0.40}$ exp $(-24.4$ kcal mol^{-1}/RT) s^{-1} were derived at 200–300 K for the direct and backward reactions of $CF_2(OH)CF_2OONO_2$, while for $CF_3CF_2OONO_2$, the expressions $1.01 \times 10^{-12}\,(T/300)^{0.39}$ cm^3 molecule^{-1} s^{-1} and $1.05 \times 10^{16}\,(T/300)^{0.44}$ exp$(-23.0$ kcal mol^{-1}/RT) s^{-1} were obtained. A decomposition lifetime profile was derived for $CF_2(OH)CF_2OONO_2$, indicating that it could act as transport and reservoir of $CF_2(OH)CF_2OO$ and NO_2 in the stratosphere.

1. Introduction

Peroxynitrates ($ROONO_2$) are formed in the atmospheric degradation processes of hydrocarbons. Due to their thermal stability, they act as temporary reservoirs of peroxy radicals, ROO, and NO_2 [1–6]. Thus, they may contribute to the transport of the above species over long distances from polluted to unpolluted areas [4,7].

In particular fluorinated peroxynitrates were postulated as important intermediates in the degradation of fluorinated compounds used as solvents, cleaning agents, etc. [8–13]. A new fluorinated peroxynitrate, $CF_2(OH)CF_2OONO_2$, was proposed as a product in the gas-phase reaction of C_2F_4 with the radicals OH [14]. This new compound was recently characterized from a structural and thermochemistry point of view [15]. However, no kinetic information is available to date.

Atmospheric peroxynitrate reactions depend on reached altitudes and nature of the involved peroxynitrate [16–18]. One possible loss process is the thermal unimolecular decomposition where $ROO–NO_2$ bond fission occurs [9–11,18,19]. To date, a number of kinetic information is available for both acyl and alkyl fluoroperoxynitrates [8,11,20–23]. These compounds are potentially important intermediates in some atmospheric reactions [20].

In this work, a theoretical kinetics study of the temperature and pressure dependence of the recombination reaction (1)

$$CF_2(OH)CF_2OO + NO_2 \rightarrow CF_2(OH)CF_2OONO_2, \quad (1)$$

and of the reverse thermal decomposition process (-1)

$$CF_2(OH)CF_2OONO_2 \rightarrow CF_2(OH)CF_2OO + NO_2. \quad (-1)$$

for the first time is reported. Rate coefficients were derived employing the SACM/CT (statistical adiabatic channel model/classical trajectory) approach [24,25] and unimolecular reaction rate theories on quantum-chemical potentials. In addition, for comparative purposes, similar high-pressure limit calculations were carried out for the related peroxynitrate $CF_3CF_2OONO_2$,

$$CF_3CF_2OO + NO_2 \rightarrow CF_3CF_2OONO_2, \quad (2)$$

and

$$CF_3CF_2OONO_2 \rightarrow CF_3CF_2OO + NO_2. \quad (-2)$$

2. Computational details

Potential energy curves for both peroxynitrates at different O–N bond distances along the minimum energy path were derived from quantum chemical calculations. To this end, the hybrid B3LYP density functional [26–28] coupled with the extended 6-311++G (3df,3pd) basis set [29] and the model chemistries G3(MP2)B3 [30,31] and G4(MP2) [32] were employed. The G3(MP2)B3 model is a variation of G3(MP2) method in which the optimized molecular structure and zero point energies (whose harmonic vibrational

E-mail address: mbadenes@inifta.unlp.edu.ar

http://dx.doi.org/10.1016/j.cplett.2017.01.064
0009-2614/

frequencies are scaled by a factor 0.96) are derived from B3LYP/6-31G(d) instead of from MP2(FULL)/6-31G(d) and HF/6-31G(d) calculations, respectively. This variation has an average absolute deviation of 1.25 kcal mol^{-1} [30,31]. The G4(MP2) method provides results with an average absolute deviation slightly smaller, 1.04 kcal mol^{-1} [32]. This method uses B3LYP/6-31G(2df,p) optimized geometries and zero point energies (with a scale factor of 0.9854), and provides CCSD(T, full) energy values with an extrapolated complete basis set [32].

The optimized molecular parameters, rotational constants, and harmonic vibrational frequencies of the most stable conformations of both peroxynitrates and the related peroxyradicals were estimated in a previous work at the same levels of theory [15]. All calculations were performed with the Gaussian 09 program package [33].

3. Results and discussion

3.1. Potential energy curves and dissociation energies

Estimations of the high-pressure rate coefficients can be performed from a quantum-chemical characterization of the isotropic and anisotropic potential of the reactions. To evaluate the isotropic part, the ROO–NO_2 potential along the reaction coordinate was calculated by scanning the O–N bond distance from the equilibrium value to 2.92 Å, while all the remaining geometrical parameters were fully optimized. Both peroxynitrates present similar equilibrium O–N bond distances of 1.538 and 1.547 Å for $CF_2(OH)CF_2$-$OONO_2$ and $CF_3CF_2OONO_2$, respectively, at the B3LYP/6-311++G (3df,3pd) level [15]. Different quantum-chemicals methods, such as B3LYP/6-311++G(3df,3pd), G3(MP2)B3 and G4(MP2) were employed for electronic potential calculations. In Figs. 1 and 2 a comparison among the obtained results is presented. As can be seen, B3LYP/6-311++G(3df,3pd) calculations give an unrealistic approach with values much larger than *ab initio* methods when the O–N distance increase. In fact, for O–N bond distances above 2.3 Å, the calculated energies exceed the dissociation energy derived from the values corresponding to the separated fragments. A similar behavior has been observed for the FC(O)OOO(O)CF, FS(O_2)OOO(O_2)SF and FC(O)OOO(O_2)SF fluorinated trioxides [34]. By contrast, G3(MP2)B3 and G4(MP2) results exhibit a more reasonable shape. They show a smooth energy profile, as frequently observed in simple bond fission reactions. Because the G4(MP2) method has average absolute deviation smaller than G3(MP2)B3, it was selected for use in the kinetic calculations.

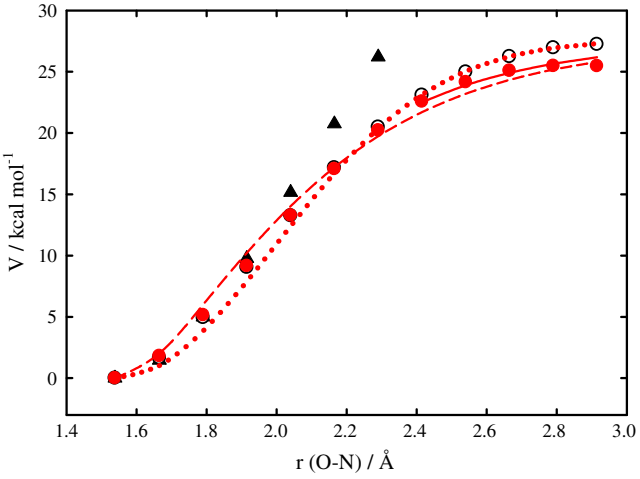

Fig. 1. Dependence of the electronic potential of $CF_2(OH)CF_2OONO_2$ on the O–N bond distance at different levels of theory. Triangles: B3LYP/6-311++G(3df,3pd). Open circles: G3(MP2)B3. Filled circles: G4(MP2). Solid line: Morse potential with β = 2.67 $Å^{-1}$. Dashed line: Morse potential with β = 2.49 $Å^{-1}$. Dotted line: Morse potential with β = 2.37 $Å^{-1}$ (see text).

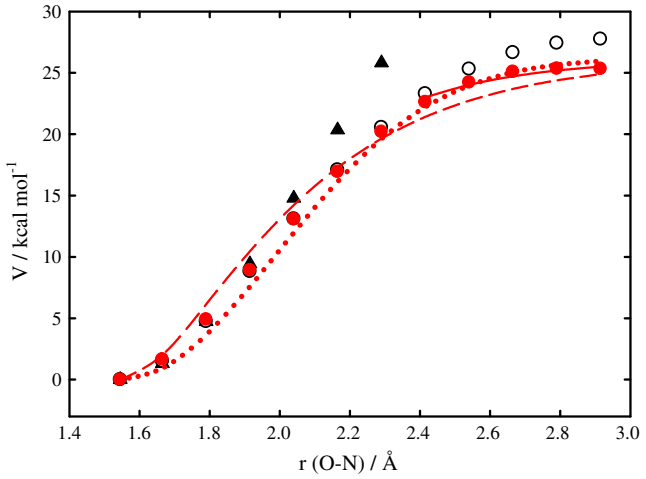

Fig. 2. Dependence of the electronic potential of $CF_3CF_2OONO_2$ on the O–N bond distance at different levels of theory. Triangles: B3LYP/6-311++G(3df,3pd). Open circles: G3(MP2)B3. Filled circles: G4(MP2). Solid line: Morse potential with β = 3.19 $Å^{-1}$. Dashed line: Morse potential with β = 2.70 $Å^{-1}$. Dotted line: Morse potential with β = 2.49 $Å^{-1}$ (see text).

The SACM/CT approach uses the standard Morse function for the minimum energy path of the reaction,

$$V = D_e[1 - \exp(-\beta(r - r_e)]^2. \quad (3)$$

In this expression, β is the Morse parameter, D_e is the dissociation energy and r_e is the equilibrium bond length. The Morse parameter can be calculated from the D_e values and the equilibrium force constants for the O–N stretching modes $F_{O\text{-}N}$, as $\beta = (F_{O\text{-}N}/2D_e)^{1/2}$. Alternatively, the Morse parameter can be derived from the *ab initio* potentials calculated here, when they are compared with a representation by Eq. (3). The $CF_2(OH)CF_2OO$–NO_2 dissociation energy was derived from enthalpies of formation at 298 K of $CF_2(OH)CF_2OONO_2$ (−265.6±2 kcal mol^{-1}) and $CF_2(OH)$ CF_2OO (−248.6±2 kcal mol^{-1}) species, such as estimated in a previous work at the G3(MP2)B3 and G4(MP2) levels of theory from balanced isodesmic reactions [15]. For this, the above enthalpies were transformed as usual to 0 K, using H°(298 K)–H°(0 K) contributions of $CF_2(OH)CF_2OONO_2$ and $CF_2(OH)CF_2OO$ calculated at the B3LYP/6-311++G(3df,3pd) level of theory, and the H°(298 K)–H °(0 K) values corresponding to fluorine, carbon, oxygen, hydrogen and nitrogen atoms of 1.05, 0.25, 1.04, 1.01 and 1.04 kcal mol^{-1} given in Ref. [35]. Thus, in combination with the enthalpy of formation at 0 K of NO_2 (8.79 ± 0.02 kcal mol^{-1} [36]), an enthalpy of dissociation at 0 K, ΔH^o_{0K}, of 24.4 kcal mol^{-1} was obtained. Then, the D_e value was calculated as $D_e = \Delta H^o_{0K} + \Delta ZPE$ = 27.6 kcal mol^{-1}, employing ZPE values from the B3LYP/6-311++G(3df,3pd) harmonic vibrational frequencies [15].

As Fig. 1 shows, the G4(MP2) potential can be acceptably fitted with a Morse function with the described value for D_e and a β value of 2.49 $Å^{-1}$ (dashed line). However, the more relevant part of the radial potential corresponds to regions of high energy located at long interfragment distances, where the Morse potential gives a poorer approach. This part of the potential can be more satisfactorily reproduced with a β parameter of 2.67 $Å^{-1}$ for bond distances above 2.4 Å (solid line). As expected, a smaller β parameter of 2.37 $Å^{-1}$ was derived with the D_e value and the equilibrium force constant for the O–N stretching mode (of 2.15 mdyn $Å^{-1}$ at the

B3LYP/6-311++G(3df,3pd) level [15]). Fig. 1 shows that this potential departs markedly from the *ab initio* potentials.

A similar treatment was performed for the $CF_3CF_2OO–NO_2$ potential. An enthalpy of dissociation at 0 K of 23.0 kcal mol^{-1} was derived from average enthalpies of formation at 298 K of $CF_3CF_2OONO_2$ (−268.2±2 kcal mol^{-1}) and CF_3CF_2OO (−252.6±2 kcal mol^{-1}) at the G3(MP2)B3 and G4(MP2) levels [15]. Therefore, $D_e = \Delta H^o_{0K} + \Delta ZPE = 26.2$ kcal mol^{-1}. Fig. 2 shows the fits carried out according to the three above approaches. The G4(MP2) curve exhibits similar shape that the calculated for $CF_2(OH)CF_2OONO_2$. The region of large $CF_3CF_2OO–NO_2$ bond distances is slightly underestimated when it is completely fitted with $\beta = 2.70$ $Å^{-1}$, but it is appropriately reproduced above 2.4 Å with a $\beta = 3.19$ $Å^{-1}$.

Unfortunately, the transitional modes of both peroxynitrates are strongly coupled and it becomes impossible the calculation of the single switching functions along the reaction coordinate. Therefore, a standard value of 0.5 for the ratio between the anisotropy and Morse parameters, α/β, was employed [37].

3.2. High-pressure limit recombination rate coefficients $k_{rec,\infty}$

The high-pressure rate coefficients for the decomposition and formation reactions were theoretically estimated employing SACM/CT calculations on *ab initio* electronic potentials described in the previous section [24,25]. This is an appropriate procedure to treat bond forming reactions with potential energy profiles without barriers, as calculated for $CF_2(OH)CF_2OONO_2$ and $CF_3CF_2OONO_2$ (Figs. 1 and 2). In this work, the combination between two quasi-linear rotors (ROO and NO_2 radicals) to form a nonlinear adduct was considered.

The limiting high-pressure rate coefficient for the recombination reaction, $k_{rec,\infty}$, can be expressed as the product between the thermal rigidity factor, f_{rigid}, and the phase space theory rate coefficient, $k^{PST}_{rec,\infty}$ [37,38]

$$k_{rec,\infty} = f_{rigid} k^{PST}_{rec,\infty}. \quad (4)$$

The anisotropy of the potential energy surface is taken into account by the thermal rigidity factor, and the phase space theory rate coefficient provides an upper bound to the rate coefficients. $k^{PST}_{rec,\infty}$ can be calculated using the expression [24]

$$k^{PST}_{rec,\infty} = f_e f_{sym} \left(\frac{8\pi kT}{\mu}\right)^{1/2} \left(\frac{\alpha_1 + \alpha_2 X + \alpha_3 X^2}{\beta^2}\right). \quad (5)$$

Here, $X = \ln(kT/D_e) - \beta r_{CM} + 4$ and the parameters $\alpha_1 = 31.153$, $\alpha_2 = -18.158$ and $\alpha_3 = 0.8685$ were taken from Table 3 of Ref. [24]. In Eq. (5), μ denotes the collisional reduced mass (35.15 and 35.26 g mol^{-1} for $CF_2(OH)CF_2OONO_2$ and $CF_3CF_2OONO_2$, respectively), $f_e = 1/4$ represents the electronic degeneracy factor, f_{sym} is a stoichiometric coefficient (1/2 for identical rotors, or 1 if the rotors are different) and r_{CM} is the distance between the centers of mass of the two combining radicals (4.11 and 4.03 Å for $CF_2(OH)CF_2OONO_2$ and $CF_3CF_2OONO_2$, respectively). Using the above D_e and β values, rate coefficients of $k^{PST}_{rec,\infty} = 1.5 \times 10^{-10}$ and 1.3×10^{-10} cm^3 $molecule^{-1}$ s^{-1} were obtained at 300 K for reactions (1) and (2).

Following the SACM/CT, f_{rigid} for $\alpha/\beta = 0.5$, can be estimated as [24]

$$f_{rigid} \approx \left[1 - 2.3C(\beta r_{CM})^{1/2} \exp\left(\frac{X-4}{2.044}\right)\right][1 + 0.75Z + Z^4]^{-1/4}, \quad (6)$$

where $Z = (dC)^n$ and $C = \{\{2\varepsilon_s^2\varepsilon_a^2\varepsilon_t^2/[B_1B_2(B_1+B_2)]\}^{1/3}\}/2D_e$ [25]. The angular dependence of f_{rigid} is accounted for the parameters $n = 1 - 0.5\sin^2\theta + \sin^4\theta$ and d (see below), where the angle between the rotors is denoted by θ. As for other polyatomic + polyatomic reactions [34,39–41], in reaction (1), the peroxynitrate $CF_2(OH)CF_2$-$OONO_2$ was assumed formed by the quasi-linear rotors $CF_2(OH)CF_2$-OO and NO_2. For the $CF_2(OH)CF_2OO$ radical one of the inertial axis was considered as the axis of the rotor, while the C_{2v} axis was assimilated to the rotor axis for NO_2. In that context, an average angle θ of 55° was determined. A similar treatment for CF_3CF_2-$OONO_2$ leads to a value of $\theta = 54°$.

In the above C expression, ε_s, ε_a and ε_t are the adduct vibrational frequencies for the symmetrical and asymmetrical deformation modes and for the torsion motion; and B_1 and B_2 are the average of the smallest rotational constants of the rotors ROO and NO_2 (listed in Table 1). For d the following equation was employed [25]

$$\begin{aligned} d = {} & c_1 + c_2\sin^2\theta + \frac{c_3}{\sin^2\theta} \\ & + \left[\left(\frac{\varepsilon_a}{\varepsilon_t}\right)\left(\frac{\varepsilon_s}{\varepsilon_t}\right)\right]^{2/3}\left(c_4 + c_5\sin^2\theta + \frac{c_6}{\sin^2\theta}\right) \\ & + \left(\frac{\varepsilon_a}{\varepsilon_t}\right)^2\cos^2\theta\left(c_7 + c_8\sin^2\theta + \frac{c_9}{\sin^2\theta}\right) \\ & + \left(\frac{\varepsilon_s}{\varepsilon_t}\right)^2\cos^2\theta\left(c_{10} + c_{11}\sin^2\theta + \frac{c_{12}}{\sin^2\theta}\right), \end{aligned} \quad (7)$$

with c_i parameters from Table A of the Supplementary Material [25].

Using estimated values of d = 3.22, n = 1.50 and C = 6.58, a f_{rigid} value of 0.01 was obtained for reaction (1) at room temperature. Analogously, with d = 23.69, n = 0.94 and C = 7.24, a $f_{rigid} = 0.008$ was calculated for reaction (2). As a consequence, according to expression (4), SACM/CT values of 1.5×10^{-12} and 1.0×10^{-12} - cm^3 $molecule^{-1}$ s^{-1} were, respectively, derived for $k_{rec,\infty}$ for reactions (1) and (2).

The obtained results between 200 and 300 K are summarized in Table 2 and can be represented by the following expressions

$$k_{rec,\infty}(CF_2(OH)CF_2OONO_2) = 1.53 \times 10^{-12}\left(\tfrac{T}{300}\right)^{0.37} cm^3\ molecule^{-1}\ s^{-1}$$
$$k_{rec,\infty}(CF_3CF_2OONO_2) = 1.01 \times 10^{-12}\left(\tfrac{T}{300}\right)^{0.39} cm^3\ molecule^{-1}\ s^{-1}$$

To quantify the errors inherent in the present approach, similar SACM/CT analysis of different recombination reactions were confronted with their corresponding experimental rate coefficients. For example, the ratio between calculated and experimental rate coefficients for the reactions F + FC(O)O + M → FC(O)OF + M, Cl + FC(O)O + M → FC(O)OCl + M and FSO_2 + $FS(O_2)O$ → $FS(O_2)O(O_2)$ SF, are of 1.2, 1/1.4 and 1.2, respectively [39,42,43,]. Consequently, the estimated mean error of the present results is of about a factor of 2.

3.3. High-pressure limit dissociation rate coefficients $k_{diss,\infty}$

To compare the kinetic behavior of $CF_2(OH)CF_2OONO_2$ and CF_3-CF_2OONO_2 with other peroxynitrates, their thermal decomposition rate coefficients are required, $k_{diss,\infty} = k_{rec,\infty}/K_C$. The equilibrium constant K_C was evaluated from calculated total partition functions of $ROONO_2$, ROO and NO_2 (R = $CF_2(OH)CF_2$ and CF_3CF_2). The

Table 1
Parameters employed in C calculation (in cm^{-1}) for reactions (1) and (2) [15].

Parameter	$CF_2(OH)CF_2OONO_2$	$CF_3CF_2OONO_2$
ε_s	178.3	174.8
ε_a	225.1	248.1
ε_t	74.8	73.8
B_1	0.044	0.044
B_2	0.427	0.427

Table 2
Calculated high-pressure rate coefficients for the recombination and dissociations reactions, $k_{rec,\infty}$ and $k_{diss,\infty}$, and equilibrium constant, K_C, for ROO + NO_2 ↔ $ROONO_2$ (R = $CF_2(OH)CF_2$ and CF_3CF_2).

T/K	$k^{PST}_{rec,\infty}$/cm^3 molecule^{-1} s^{-1}	f_{rigid}	$k_{rec,\infty}$/cm^3 molecule^{-1} s^{-1}	K_C/cm^3 molecule^{-1}	$k_{diss,\infty}$/s^{-1}
$CF_2(OH)CF_2OO + NO_2 \leftrightarrow CF_2(OH)CF_2OONO_2$					
200	1.32×10^{-10}	0.00997	1.31×10^{-12}	4.04×10^{-2}	3.25×10^{-11}
220	1.37×10^{-10}	0.00995	1.36×10^{-12}	1.49×10^{-4}	9.15×10^{-9}
240	1.41×10^{-10}	0.00994	1.40×10^{-12}	1.40×10^{-6}	1.00×10^{-6}
260	1.46×10^{-10}	0.00993	1.45×10^{-12}	2.74×10^{-8}	5.27×10^{-5}
280	1.50×10^{-10}	0.00992	1.49×10^{-12}	9.49×10^{-10}	1.57×10^{-3}
298	1.54×10^{-10}	0.00991	1.52×10^{-12}	6.67×10^{-11}	2.28×10^{-2}
300	1.54×10^{-10}	0.00991	1.53×10^{-12}	5.19×10^{-11}	2.94×10^{-2}
$CF_3CF_2OO + NO_2 \leftrightarrow CF_3CF_2OONO_2$					
200	1.11×10^{-10}	0.00777	8.62×10^{-13}	1.35×10^{-3}	6.37×10^{-10}
220	1.16×10^{-10}	0.00776	9.00×10^{-13}	6.85×10^{-6}	1.31×10^{-7}
240	1.20×10^{-10}	0.00775	9.30×10^{-13}	8.45×10^{-8}	1.10×10^{-5}
260	1.24×10^{-10}	0.00775	9.61×10^{-13}	2.07×10^{-9}	4.65×10^{-4}
280	1.27×10^{-10}	0.00775	9.84×10^{-13}	8.67×10^{-11}	1.13×10^{-2}
298	1.31×10^{-10}	0.00774	1.01×10^{-12}	7.11×10^{-12}	1.43×10^{-1}
300	1.31×10^{-10}	0.00774	1.01×10^{-12}	5.60×10^{-12}	1.81×10^{-1}

Table 3
Rotational constants for $ROONO_2$, ROO and NO_2 calculated at the B3LYP/6-311++G (3df,3pd) level (in cm^{-1}). R = $CF_2(OH)CF_2$ and CF_3CF_2.

Species	Rotational constants		
$ROONO_2$	0.066	0.019	0.018
ROO	0.087	0.045	0.043
NO_2	8.169	0.438	0.415

harmonic vibrational frequencies were taken from Ref. [15], the rotational constants (listed in Table 3) were calculated at the B3LYP/6-311++G(3df,3pd) level (obtained values are very similar for R = $CF_2(OH)CF_2$ and CF_3CF_2) and above values of ΔH^o_{0K} were employed (see Section 3.1).

The torsional modes were considered as internal hindered rotations. However, due to the potential energy functions for internal rotational around C–OH, C–C and C–O bonds in $ROONO_2$ and ROO are very similar, the internal rotational partition functions Q_{rotint} approximately cancel in K_C. Therefore, only the torsions about O–O and O–N bonds in $ROONO_2$ were considered [15].

The Q_{rotint} functions were calculated using the approximated Troe's expression that interpolates between the partition functions for totally restricted internal rotations, Q_{tors}, and for completely free rotors, Q_{free}, [37]

$$Q_{rotint} = Q_{tors}\left[\exp\left(-\frac{RT}{V_0}\right)\right]^{1.2} + Q_{free}\left[1-\exp\left(-\frac{RT}{V_0}\right)\right]^{1.2}, \qquad (8)$$

with $Q_{tors} = [1-\exp(-h\nu_{tors}/RT)]^{-1}$ and $Q_{free} = (2\pi I_m k/\hbar^2)^{1/2}$. The required molecular input data (rotational barrier heights V_0, reduced moments of inertia $I_m = I_A I_B/(I_A+I_B)$ and torsion values ν_{tors}) were taken from Ref. [15] and they are listed in Tables B and C of Supplementary Material.

In this way, the value 6.7×10^{-11} cm^3 molecule^{-1} was derived for K_C at 298 K for $CF_2(OH)CF_2OONO_2$ and, consequently $k_{diss,\infty} = 2.3 \times 10^{-2}$ s^{-1}. If all internal rotational modes are treated as harmonic oscillators, a K_C value of about a factor of 2 smaller is obtained. Analogously for $CF_3CF_2OONO_2$, $K_C = 7.1 \times 10^{-11}$ cm^3 molecule^{-1} and $k_{diss,\infty} = 1.4 \times 10^{-1}$ s^{-1} at 298 K. The complete set of calculated $k_{diss,\infty}$ and K_C at 200–300 K, included in Table 2, are very well represented by the following expressions

$$k_{diss,\infty}(CF_2(OH)CF_2OONO_2) = 1.79 \times 10^{16}\left(\tfrac{T}{300}\right)^{0.40}\exp\left(-\tfrac{24.4\ \text{kcal mol}^{-1}}{RT}\right)\ \text{s}^{-1}$$

$$k_{diss,\infty}(CF_3CF_2OONO_2) = 1.05 \times 10^{16}\left(\tfrac{T}{300}\right)^{0.44}\exp\left(-\tfrac{23.0\ \text{kcal mol}^{-1}}{RT}\right)\ \text{s}^{-1}$$

$$K_C(CF_2(OH)CF_2OONO_2) = 8.54 \times 10^{-29}\left(\tfrac{T}{300}\right)^{-0.03}\exp\left(\tfrac{24.4\ \text{kcal mol}^{-1}}{RT}\right)\ \text{cm}^3\ \text{molecule}^{-1}$$

$$K_C(CF_3CF_2OONO_2) = 9.67 \times 10^{-29}\left(\tfrac{T}{300}\right)^{-0.03}\exp\left(\tfrac{23.0\ \text{kcal mol}^{-1}}{RT}\right)\ \text{cm}^3\ \text{molecule}^{-1}$$

It is interesting to note that the $k_{diss,\infty}$ value estimated from the above Arrhenius expression for $CF_3CF_2OONO_2 \rightarrow CF_3CF_2OO + NO_2$ at 285 K, 2.4×10^{-2} s^{-1}, compares very well with the experimental value of 2.88×10^{-2} s^{-1}, determined from the 254–nm photolysis of $CF_3CF_2C(O)Cl$ in the presence of NO_2 and O_2 at 279–290 K [9]. In addition, the results for both peroxynitrates can be compared with the value of 4.2×10^{-2} s^{-1}, measured for $CF_3OONO_2 \rightarrow CF_3OO + NO_2$ at 298 K and near to the high-pressure limit [20].

3.4. Low-pressure limit rate coefficients and falloff curves

To extend the kinetic analysis of $CF_2(OH)CF_2OONO_2$ decomposition to the *falloff* region, the knowledge of the low-pressure limit rate coefficient $k_{diss,0}$ is necessary. This rate coefficient was estimated employing Troe's factorized formalism [44,45],

$$k_{diss,0} = \beta_c[M]Z_{LJ}\left(\frac{\rho_{vib,h}(E_0)kT}{Q_{vib}}\right)\exp\left(-\frac{E_0}{kT}\right)F_{anh}F_E F_{rot}F_{rotint}. \qquad (9)$$

In this expression, β_c is the collision efficiency which depends on intermolecular energy transfer properties, Z_{LJ} is the Lennard-Jones collision frequency between $CF_2(OH)CF_2OONO_2$ and a given bath gas M (assumed here to be He), $\rho_{vib,h}(E_0) = 2.38 \times 10^{10}$ (kcal mol^{-1})$^{-1}$ is the $CF_2(OH)CF_2OONO_2$ harmonic vibrational density of states at the threshold energy $E_0 \approx \Delta_0 H^0 = 24.4$ kcal mol^{-1}, and Q_{vib} is the vibrational partition function of this peroxynitrate. On the other hand, the $F_{anh} = 1.099$ takes into account the anharmonicity of the dissociating molecule, F_E considers the energy dependence of $\rho_{vib,h}(E_0)$, while F_{rot} and F_{rotint} factors describe the external and internal rotational effects. The evaluation of these factors was carried out employing the molecular data given in Ref. [15]. Lennard-Jones collision parameters were calculated using tabulated values of $\sigma = 2.55$ Å and $\varepsilon/k = 10$ K for He [46] and estimated values of $\sigma = 5.98$ Å and $\varepsilon/k = 266$ K for $CF_2(OH)CF_2OONO_2$, in which additivity relationships for molar volumes and molecular similitude to CF_3OONO_2 were considered [47]. The electronic potential computed at the G4(MP2) level was used for the F_{rot} estimations (see Section 3.1). $CF_2(OH)CF_2OONO_2$ presents five internal rotations around the C–OH, C–O, O–O, O–N, and C–C bonds, which were studied in a previous work [15]. The barrier heights and its

Table 4
Contributing factors to $k_{diss,0}$ for reaction $CF_2(OH)CF_2OONO_2 + He \rightarrow CF_2(OH)CF_2OO + NO_2 + He$.

T/K	Z_{LJ}/cm^3 molecule^{-1} s^{-1}	F_E	F_{rot}	F_{rotint}	Q_{vib}	β_c	$k_{diss,0}$/[He] cm^3 molecule^{-1} s^{-1}
200	5.93×10^{-10}	1.31	5.90	20.70	4.07	0.219	1.16×10^{-25}
220	6.09×10^{-10}	1.36	5.24	16.25	5.58	0.200	1.66×10^{-23}
240	6.24×10^{-10}	1.40	4.70	13.01	7.78	0.183	9.49×10^{-22}
260	6.39×10^{-10}	1.45	4.25	10.59	10.98	0.169	2.68×10^{-20}
280	6.53×10^{-10}	1.50	3.87	8.74	15.68	0.156	4.33×10^{-19}
300	6.66×10^{-10}	1.55	3.54	7.31	22.59	0.144	4.48×10^{-18}

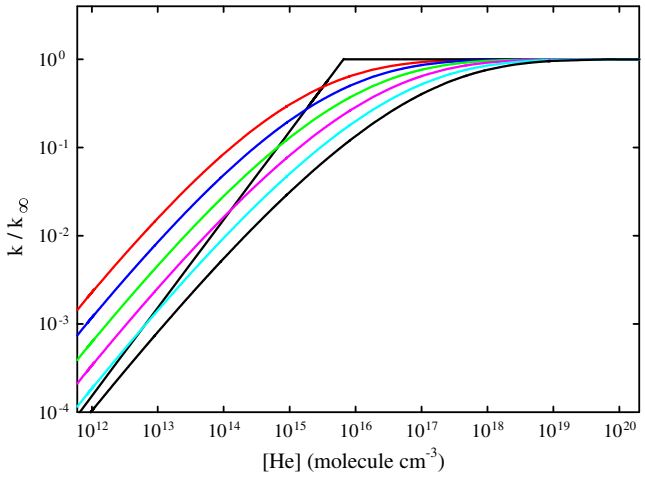

Fig. 3. *Falloff* curves for $CF_2(OH)CF_2OONO_2 + He \rightarrow CF_2(OH)CF_2OO + NO_2 + He$ at (from left to right) 200, 220, 240, 260, 280, and 300 K.

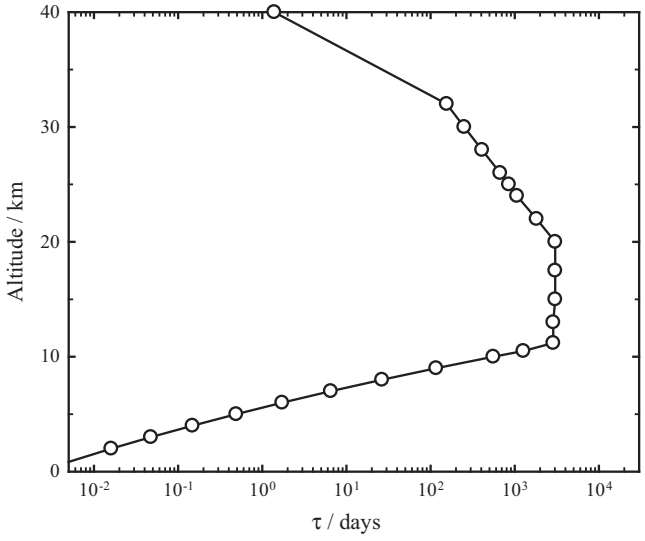

Fig. 4. Thermal atmospheric lifetimes for $CF_2(OH)CF_2OONO_2$.

corresponding reduced moments of inertia were taken from Ref. [15] and they are listed in Table B of Supplementary Material. As can be seen, rotation about C–OH bond has a small barrier height and, thus, it was considered as a free rotor. Therefore, only four internal rotations were taken into account. They were approximated as equivalent hindered rotors with average barrier heights of 8.4 kcal mol^{-1} and average reduced moments of inertia of 96.6 amu Å^2 [15].

The estimation of the different factors contributing to $k_{diss,0}$ derived between 200 and 300 K are presented in Table 4. The β_c values were calculated from the expression $-\langle\Delta E\rangle \approx F_E\ kT\ \beta_c/(1-\beta_c^{1/2})$ [44], considering that the average energy transferred in $CF_2(OH)CF_2OONO_2$–He collisions, $-\langle\Delta E\rangle \approx 75$ cm^{-1}, does not change in the narrow range of studied temperatures [46]. The obtained results can be depicted by the following expressions (with a mean error no better than a factor of 2 when the input data are sufficiently well-known [44,45])

$$k_{diss,0}(CF_2(OH)CF_2OONO_2) = [He]8.08 \times 10^{-3} \exp\left(-\frac{20.9\ \text{kcal mol}^{-1}}{RT}\right)\ \text{cm}^3\ \text{molecule}^{-1}\ \text{s}^{-1}$$

$$k_{rec,0}(CF_2(OH)CF_2OONO_2) = [He]2.45 \times 10^{-28} \left(\frac{T}{300}\right)^{-7.40}\ \text{cm}^6\ \text{molecule}^{-2}\ \text{s}^{-1}$$

where $k_{rec,0}$ equation was derived from $K_C(CF_2(OH)CF_2OONO_2)$ calculated in the previous section.

Then, to explore the pressure dependence of the $CF_2(OH)CF_2OONO_2$ decomposition reaction, the *falloff* curve was calculated. To this end, the Troe's reduced method was employed [48,49]. In this procedure, the rate coefficients are estimated as

$$k \approx k_{diss,\infty} F^{LH}(x) F(x). \quad (10)$$

In above expression, $x = k_{diss,0}/k_{diss,\infty}$, $F^{LH}(x) = x/(1+x)$ is the result of the Lindemann-Hinshelwood mechanism, and the broadening factor F(x) accounts for corrections due to the energy and total angular momentum dependences of the energized adducts and the multistep character of the collisional energy transfer. This factor is represented by [49]

$$F(x) = \frac{\left[1 + \frac{x}{x_0}\right]}{\left[1 + \left(\frac{x}{x_0}\right)^n\right]^{1/n}}, \quad (11)$$

where $n = [\ln 2/\ln(2/F_{cent})][1 - b + b(x/x_0)^q]$, $q = (F_{cent} - 1)/\ln(F_{cent}/10)$, $x_0 \approx 1$, $b \approx 0.2$, and $F_{cent} = F(x = 1)$ is the center broadening factor. The last factor can be approximated as the product between the weak and the strong collision broadening factors, $F_{cent} = F_{cent}^{WC} F_{cent}^{SC}$, where $F_{cent}^{WC} = \beta_c^{0.14}$ and $\log F_{cent}^{SC} = -(1.06 \log S_T)^{2.2}/(1 + C_1 S_T^{C_2})$, with $C_1 = 0.10 \exp(2.5 B_T^{-1} - 0.22 B_T - 6 \times 10^{-10} B_T^6)$, and $C_2 = 1.9 + 4.6 \times 10^{-5} B_T^{2.8}$ [48]. The Kassel parameters, S_T and B_T, were calculated from harmonic vibrational frequencies given in Ref. [15] and $\Delta_0 H^0 = 24.4$ kcal mol^{-1} (Section 3.1.). Estimated F_{cent} values ranged between 0.32 and 0.21 when temperature increases from 200 to 300 K. In these cases (F_{cent} values below ~0.4), the broadening factors become asymmetric and expressions (10) and (11) are preferred instead of the usual approximate representation derived from rigid-activated complex, strong-collision RRKM theory [49]. Fig. 3 shows the resulting reduced *falloff* curves at 200–300 K. The bath gas concentration corresponding to the center of the *falloff* curves, $[He]_c = k_{diss,\infty}/k_{diss,0}$ [He], is located at the intersection of the straight lines (drawn for simplicity only at 300 K). As can be observed, the $CF_2(OH)CF_2OONO_2$ decomposition reaction at atmospheric pressure (about 3.7×10^{19} molecule cm^{-3} at 200 K and 2.5×10^{19} molecule cm^{-3} at 300 K) is near to the high-pressure limit. A small *falloff* behavior is apparent at lower pressures, as

those corresponding to high altitudes on the surface of the Earth. On the other hand, for a given pressure a decrease in k/k_{∞} is observed when the temperature is increased.

3.5. Atmospheric implications

From $k_{diss,\infty}$ values presented in Section 3.3, lifetimes of about 7 and 40 s were respectively obtained for $CF_3CF_2OONO_2$ and $CF_2(OH)CF_2OONO_2$ at 298 K. The very short computed value for $CF_2(OH)CF_2OONO_2$ is smaller than the rough estimate reported in a previous work [15]. However, it reaches up to more than 1 day at temperatures close to 250 K. This value can be considered as a lower bound to the lifetime at the temperatures and pressures of the tropopause [9,20].

A more realistic estimation of the thermal lifetimes can be obtained from the unimolecular *falloff* curves of Section 3.4. Fig. 4 shows the profile calculated for $CF_2(OH)CF_2OONO_2$. The resulting lifetimes are slightly larger than those obtained for $CF_3CF_2OONO_2$ [9]. As can be seen, the thermal lifetimes are longer than 100 days at stratospheric altitudes ranging from 9 to 30 km (where the temperatures are lower than 250 K), just where the ozone layer is located. Beyond 30 km, the thermal lifetimes decrease. Therefore, the $CF_2(OH)CF_2OONO_2$ could act as transport and reservoir of $CF_2(OH)CF_2OO$ and NO_2 radicals. Finally, a comparison between thermal and photochemical lifetimes would be required to decide which of both processes controls the atmospheric lifetime.

4. Conclusions

SACM/CT kinetics calculations on an G4(MP2) electronic potential allowed to derive kinetic properties for the formation and thermal decomposition reaction of the new peroxynitrate $CF_2(OH)CF_2OONO_2$ for the first time. Additionally, kinetic information for the related peroxynitrate $CF_3CF_2OONO_2$ are also reported. Values of $k_{rec,\infty}$ of 1.5×10^{-12} and 1.0×10^{-12} cm^3 $molecule^{-1}$ s^{-1} were derived at room temperature for $CF_2(OH)CF_2OONO_2$ and $CF_3CF_2OONO_2$, respectively. While for $k_{diss,\infty}$, values of 2.3×10^{-2} and 1.4×10^{-1} s^{-1} were obtained at the same temperature. Last results allow estimating thermal lifetimes of 40 and 7 s respectively, suggesting that $CF_2(OH)CF_2OONO_2$ would be transported in the atmosphere. Additionally, the kinetic analysis of $CF_2(OH)CF_2OONO_2$ decomposition was extended to the *falloff* region.

Acknowledgements

This research project was supported by the Universidad Nacional de La Plata, the Consejo Nacional de Investigaciones Científicas y Técnicas CONICET [PIP-1134] and the Agencia Nacional de Promoción Científica y Tecnológica [PICT-478, PICT-2425].

Appendix A. Supplementary material

Supplementary data associated with this article can be found, in the online version, at http://dx.doi.org/10.1016/j.cplett.2017.01.064.

References

[1] E.R. Stephens, Adv. Environ. Sci. Technol. 1 (1969) 119.
[2] J.M. Roberts, Atmos. Environ. A 24 (1990) 243.
[3] T. Nielsen, U. Samuelsson, P. Grennfelt, E.L. Thomsen, Nature 293 (1981) 553.
[4] H.B. Singh, Environ. Sci. Technol. 21 (1987) 320.
[5] F. Kirchner, A. Mayer-Figge, F. Zabel, K.H. Becker, J. Chem. Kinet. 31 (1999) 127.
[6] T.J. Wallington, J. Sehested, O.J. Nielsen, Chem. Phys. Lett. 226 (1994) 563.
[7] H.B. Singh, L.J. Salas, W. Viezee, Nature 321 (1986) 588.
[8] J.Q. Xiongt, R.W. Carr, J. Phys. Chem. 98 (1994) 9811.
[9] A.G. Bossolasco, F.E. Malanca, G.A. Argüello, J. Photochem. Photobiol. A: Chem. 231 (2012) 45.
[10] A.G. Bossolasco, F.E. Malanca, M.A. Burgos Paci, G.A. Argüello, J. Phys. Chem. A 116 (2012) 9904.
[11] A.G. Bossolasco, J.A. Vila, M.A. Burgos Paci, F.E. Malanca, G.A. Argüello, Chem. Phys. 441 (2014) 11.
[12] R. Kopitzky, H. Willner, H.-G. Mack, A. Pfeiffer, H. Oberhammer, Inorg. Chem. 37 (1998) 6208.
[13] L. Yao, L. Du, M. Ge, D. Wang, J. Chem. Phys. 126 (2007) 184301.
[14] G. Acerboni, N.R. Jensen, B. Rindone, J. Hjorth, Chem. Phys. Lett. 309 (1999) 364.
[15] R.I. Delvalle Mongelós, M.P. Badenes, Comput. Theor. Chem. 1062 (2015) 65.
[16] J.M. Roberts, PAN and related compounds, in: R. Koppmann (Ed.), Volatile Organic Compounds in the Atmosphere, Blackwell Publishing Ltd., Oxford, UK, 2007.
[17] R.M. Ravelo, J.S. Francisco, J. Phys. Chem. A 2008 (1981) 112.
[18] M.P. Badenes, L.B.B. Bracco, C.J. Cobos, J. Phys. Chem. A 115 (2011) 7744.
[19] M.P. Badenes, C.J. Cobos, J. Mol. Struct.: Theochem. 856 (2008) 59.
[20] A. Mayer-Figge, F. Zabel, K.H. Becker, J. Phys. Chem. 100 (1996) 6587.
[21] D. Henao, F.E. Malanca, M.S. Chiappero, G.A. Argüello, J. Phys. Chem. A 117 (2013) 3625.
[22] R. Kopitzky, M. Beuleke, G. Balzer, H. Willner, Inorg. Chem. 1997 (1994) 36.
[23] F.E. Malanca, M.S. Chiappero, G.A. Argüello, J. Photochem. Photobiol. A: Chem. 184 (2006) 212.
[24] A.I. Maergoiz, E.E. Nikitin, J. Troe, V.G. Ushakov, J. Chem. Phys. 108 (1998) 9987.
[25] A.I. Maergoiz, E.E. Nikitin, J. Troe, V.G. Ushakov, J. Chem. Phys. 117 (2002) 4201.
[26] A.D. Becke, J. Chem. Phys. 98 (1993) 5648.
[27] A.D. Becke, Phys. Rev. A 38 (1988) 3098.
[28] C. Lee, W. Yang, R.G. Parr, Phys. Rev. B 37 (1988) 785.
[29] M.J. Frisch, J.A. Pople, J.S. Binkley, J. Chem. Phys. 80 (1984) 3265 (and references therein).
[30] A.G. Baboul, L.A. Curtiss, P.C. Redfern, K. Raghavachari, J. Chem. Phys. 110 (1999) 7650.
[31] L.A. Curtiss, P.C. Redfern, V. Rassolov, G. Kedziora, J.E. Pople, J. Chem. Phys. 114 (2001) 9287.
[32] L.A. Curtiss, P.C. Redfern, K. Raghavachari, J. Chem. Phys. 127 (2007) 124105.
[33] M.J. Frisch et al., Gaussian 09, Revision A.02, Gaussian Inc, Wallingford, CT, 2009.
[34] M.P. Badenes, M.E. Tucceri, C.J. Cobos, Chem. Phys. Lett. 616–617 (2014) 81.
[35] J.W. Ochterski, Thermochemistry in Gaussian, <http://www.gaussian.com/g_whitepap/thermo.htm>.
[36] S.P. Sander, R.R. Friedl, J.R. Barker, D.M. Golden, M.J. Kurylo, P.H. Wine, J.P.D. Abbatt, J.B. Burkholder, C.E. Kolb, G.K. Moortgat, R.E. Huie, V.L. Orkin, Chemical Kinetics and Photochemical Data for Use in Atmospheric Studies, NASA/JPL, Data Evaluation, JPL Publication 06-2 Evaluation No. 17, NASA, Pasadena, CA, June 1, 2011. <http://jpldataeval.jpl.nasa.gov>.
[37] C.J. Cobos, J. Troe, J. Chem. Phys. 83 (1985) 1010.
[38] J. Troe, J. Chem. Phys. 75 (1981) 226.
[39] M.E. Tucceri, A.E. Croce, C.J. Cobos, Chem. Phys. Lett. 404 (2005) 232.
[40] C.J. Cobos, A.E. Croce, K. Luther, J. Troe, J. Phys. Chem. A 114 (2010) 4747.
[41] C.J. Cobos, A.E. Croce, K. Luther, L. Soelter, E. Tellbach, J. Troe, J. Phys. Chem. A 117 (2013) 11420.
[42] M.P. Badenes, A.E. Croce, C.J. Cobos, Phys. Chem. Chem. Phys. 6 (2004) 747.
[43] M.P. Badenes, A.E. Croce, C.J. Cobos, J. Phys. Chem. A 110 (2006) 3186.
[44] J. Troe, J. Chem. Phys. 66 (1977) 4758.
[45] J. Troe, J. Phys. Chem. 83 (1979) 114.
[46] H. Hippler, J. Troe, H.J. Wendelken, J. Chem. Phys. 78 (1983) 6709.
[47] NIST Chemistry WebBook. NIST Standard Reference Database Number 69. <http://webbook.nist.gov/chemistry>.
[48] J. Troe, Ber. Bunsenges. Phys. Chem. 87 (1983) 161.
[49] J. Troe, V.G. Ushakov, Z. Phys. Chem 228 (2014) 1.